

Synthesis, DNA Binding Studies, Antimicrobial Activities, and Molecular Docking Investigations of Schiff Base Ligand and its Cu(II) and Ni(II) Complexes

Prema Mahadeva¹, Revanasiddappa Hosakere Doddarevanna^{1,*} 

¹ Department of Studies in Chemistry, University of Mysore, Manasagangotri, Mysuru-570006, India

* Correspondence: hdrevasiddappa@yahoo.com; premam@chemistry.uni-mysore.ac.in;

Received: 9.12.2023; Accepted: 7.07.2024; Published: 20.12.2025

Abstract: Herein, computational molecular docking, UV-visible, and fluorescence spectroscopic techniques have been used to explore the DNA, p53 cancer mutant protein and Cu, Zn-SOD binding interaction of the ligand (HL) and its Cu(II) and Ni(II) complex, [Cu(HL)₂] x 2H₂O (B-1) and [Ni(HL)₂] x 2H₂O (B-2). The compounds were further tested for antimicrobial activities. The DNA-binding studies were carried out using electronic absorption and fluorescence techniques. The spectral experiments revealed that the metal complexes exhibited higher binding constants. Docking analysis showed that the ligand HL interacted with DNA via intercalation, while its complexes displayed a mixed mode of interactions, and the Cu(II) complex displayed greater binding affinity for DNA and the p53 cancer mutant protein. The copper complex showed good antibacterial activity against the tested strains. The Cu and Ni complexes exhibited greater antioxidant activities with lower IC₅₀ values.

Keywords: fluorescence; CT-DNA; BSA; molecular docking; enhancement; quenching.

© 2025 by the authors. This article is an open-access article distributed under the terms and conditions of the Creative Commons Attribution (CC BY) license (<https://creativecommons.org/licenses/by/4.0/>), which permits unrestricted use, distribution, and reproduction in any medium, provided the original work is properly cited. The authors retain copyright of their work, and no permission is required from the authors or the publisher to reuse or distribute this article, as long as proper attribution is given to the original source.

1. Introduction

The history of metformin started in Europe, where the plant “French lilac” or goat’s rue” was first used to extract metformin. This medicinal plant was used to treat the symptoms of diabetes mellitus in humans and to increase milk production in cattle. In the late 1940s, people began focusing on metformin after several reports showed its ability to lower blood sugar levels in humans. In 1957, the French physician Jean Sterne published the first clinical trial of metformin for the treatment of diabetes [1]. Metformin hydrochloride is an N, N-dimethyl biguanide, a glucose-lowering agent. Metformin (MF) has been widely used to control noninsulin-dependent diabetes mellitus. Diabetes is a group of metabolic disorders characterized by high blood sugar levels over a long time; this results in symptoms such as increased thirst and hunger as well as frequent urination. Metformin improves liver sensitivity to insulin, decreases hepatic glucose production, increases insulin absorption, and increases glucose uptake by peripheral tissues; therefore, it is effective in treating loss of appetite, which leads to weight loss. Besides its use as an antidiabetic, metformin [MF] has been shown to have anticancer and anti-aging effects and to reduce the risk of cardiovascular disease. Although other biguanide drugs induce lactic acidosis, metformin does not; however, nearly 30% of patients on metformin therapy suffer from gastrointestinal side effects. There is much interest

in MF and its transition metal complexes, which are cationic. Given the potential importance of Schiff bases in coordination chemistry [2-11]. Ever since metformin was developed as an antihyperglycemic drug, its efficacy, safety profile, metabolic actions, and ability to be combined with other antidiabetic agents have been evaluated and are widely prescribed by clinicians for the treatment of diabetes mellitus. [12]. Metformin remains the ideal drug for the treatment of Type-2 diabetes mellitus due to its proven safety record, weight neutrality, possible cardiovascular benefits, and low cost. Although metformin is efficacious in lowering blood glucose levels, many patients with Type-2 diabetes are not adequately controlled when metformin is prescribed as a mono-therapy [13]. Recently, the Cr(III)-MF complex, as a diabetic drug model, was synthesized and has shown great efficacy as an antidiabetic drug [14].

Thus, the authors have reported the synthesis of a new Schiff base ligand (HL) derived from metformin conjugated with a 3-ethoxy-4-hydroxybenzaldehyde. The synthesis of the ligand is shown in Scheme 1. The structure of the ligand (HL) was confirmed by mass spectra, $^1\text{H-NMR}$, $^{13}\text{C-NMR}$, and FT- IR spectra.

2. Materials and Methods

2.1. Materials.

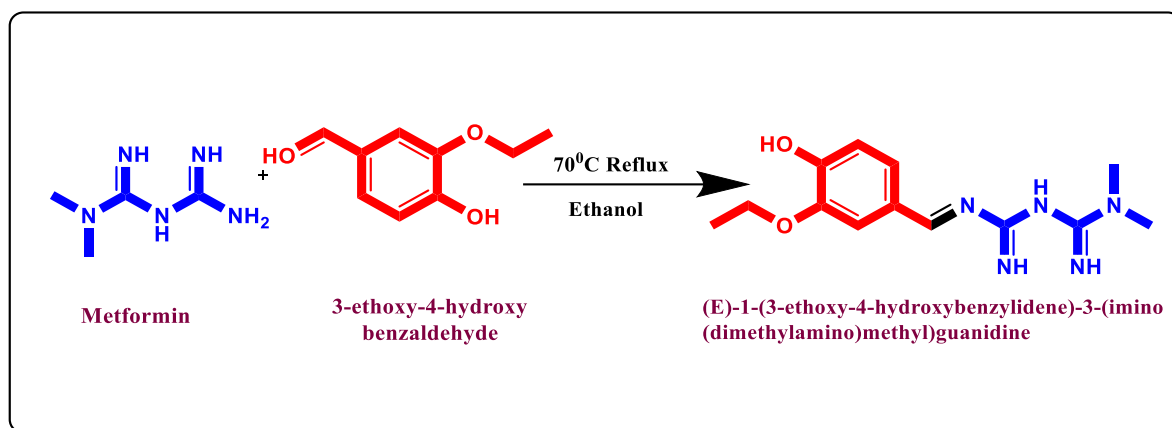
Metformin, 3-ethoxy-4-hydroxy benzaldehyde, ethanol, DMSO, Tris HCl buffer, calf thymus DNA (highly polymerized, stored at 4°C) CT- CT-DNA, DPPH, and ascorbic acid were purchased from Sigma Corp., and they were used as supplied.

2.2. Methods and instrumentation.

The melting point determination was uncorrected in an open capillary tube using a precision digi-melting point apparatus. Mass spectra of the synthesized compounds were recorded using a Shimadzu LC-MS-2010 EV spectrometer. The ^1H and ^{13}C NMR spectra were recorded using a VNMR-400 “Agilent-NMR” spectrometer, and chemical shifts were reported in ppm with residual DMSO as the reference. FT-IR spectra were recorded on a Perkin-Elmer Spectrum Version 10.03.09 spectrophotometer in the 4000-400 cm^{-1} range. Microanalysis (C, H, N, O, and M) was performed on a Perkin-Elmer analyzer. UV-visible spectra were recorded using a DU 730 Spectrophotometer (S/N 1333105, Instrument version 1.05) with a diode-array detector. Fluorescence spectra were measured on a Varioskan Flash (4.00.53 Thermo Scientific USA) using 96-well plates. The excitation and emission slits were set at 5 nm each. The wavelength increment was set at 2 nm. Electron spin resonance (ESR) spectra were recorded using a JEOL JES-TE100 ESR Spectrometer in DMSO solution at LNT in the solid state on X-band at 9.13 GHz under a magnetic field of 300 mT.

2.2.1. Synthesis of ligand.

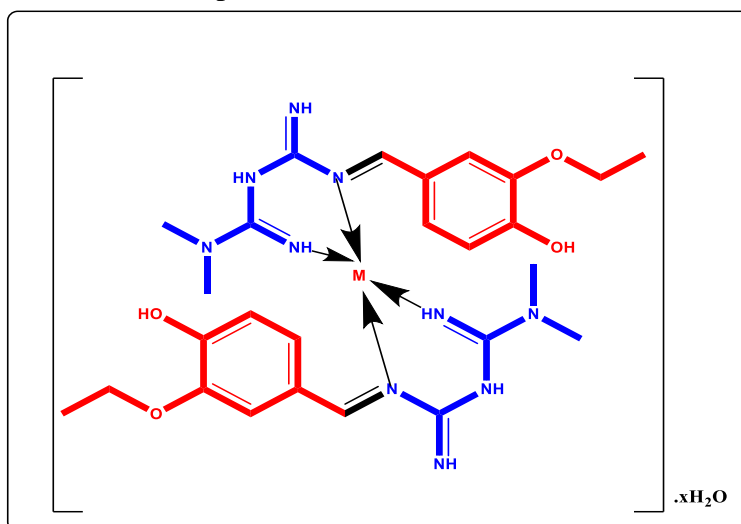
The ligand HL was synthesized by 1:1 condensation of metformin with 3-ethoxy-4-hydroxy benzaldehyde. A solution of metformin (0.15 g) in 8 mL of hot ethanol was refluxed with 3-ethoxy-4-hydroxy benzaldehyde (0.15 g) in 5 mL of ethanol for 5 h at 70°C. After cooling to room temperature, the pink crystals formed were washed with ethanol and dried. The completion of the reaction was monitored using TLC plates[n-hexane: ethyl acetate=8:2]. A pure synthesized compound was obtained from continuous recrystallization. The synthetic route is depicted in Scheme 1.



Scheme 1. Synthesis of Schiff base ligand (HL).

2.2.2. Synthesis of metal complexes [B-1 and B-2].

The ligand (HL, 2.0 mmol) was dissolved in ethanol by heating and intensive stirring. To the warm suspension, the warm ethanol solution of copper(II) chloride dihydrate (1.0 mmol) was added dropwise. The resulting mixture was kept under reflux over a water bath for 4 h at 80°C. The solvent was removed, and the resulting complex (B-1) was used directly for further processing. Similarly, the complex B-2 was prepared using nickel(II) chloride hexahydrate. The proposed structure of the complex is shown in Scheme 2.



Scheme-2. General scheme for the synthesis of metal complexes [B-1 to B-2] (M= Cu and Ni).

2.3. Bioassay studies.

2.3.1. Molecular docking methodology alter for B-1 and B-2.

Crystal structures of DNA (1BNA), the p53 cancer mutant protein (4L09), and Cu, Zn-SOD (1CB4) were downloaded from the Protein Data Bank (www.rcsb.org) and used for docking studies. The synthesized compounds were drawn using ChemDraw software, and energy minimization was computed using PyRx. The DNA, p53 cancer mutant protein, and Cu, Zn-SOD were prepared in Biovia Discovery Studio by adding hydrogen to the polar atoms, and the valencies of the metal ions were optimized [15]. The water molecules and substrate were deleted. A grid for DNA [with the dimension (22.7058 x 23.8346 x 38.3763 Å for HL; 23.2378 x 23.9765 x 38.4598 Å for B-1; 22.4991 x 23.1487 x 37.8898 Å for B-2, respectively), for p53 cancer mutant protein (with the dimension of 71.1348 x 90.0226 x 25.0000 Å for HL;

73.1587 x 93.8976 x 28.4513 Å for B-1; 72.5499 x 91.2987 x 26.2365 Å for B-2, respectively) and for Cu, Zn-SOD (with the dimension 70.6320 x 51.6335 x 18.4356 Å for HL; 72.5367 x 51.8987 x 18.8978 Å for B-1; 72.5379 x 52.2348 x 19.2485 Å for B-2, respectively) were prepared. The compounds were evaluated based on glide scoring [16].

2.3.2. Spectrophotometric titrations.

Absorption spectra were recorded on a UV-visible spectrophotometer using 3 mL quartz cuvettes. The DNA binding experiments were carried out at physiological pH (7.4) and temperature (34°C) by keeping the constant complex concentration with varied concentrations of CT-DNA from 1 – 7 µM. The concentration of the stock solution of CT-DNA was fixed as 10⁻⁴ M, and UV-visible spectra were recorded. The binding constant was calculated using the eq (1)

$$\frac{[DNA]}{\epsilon a - \epsilon b} = \frac{[DNA]}{\epsilon b - \epsilon f} + \frac{1}{K_b(\epsilon b - \epsilon f)} \quad (1)$$

Where [DNA] is the concentration of CT-DNA. ϵa is the apparent extinction coefficient and ϵf is the extinction coefficient of the free complex in the absence of DNA, ϵb is the extinction coefficient of the complex with bound DNA, and K_b is the binding constant. [17].

2.3.3. Antioxidant activity.

Each sample's free radical scavenging activity was measured using a DPPH assay. The DPPH (0.2 mM) methanolic solution was prepared and incubated for 2 hours before the analysis [18]. 2mg of the ligand (HL) and its metal complexes were dissolved in methanol. 1 mL of DPPH was added to different volumes of ligand and metal complexes, and the mixtures were made up to 4 mL with the solvent. The samples were stored in the dark at room temperature. After 30 minutes, the absorbance was measured at 517 nm. Ascorbic acid was taken as the standard and control. The lower absorbance is indicative of higher scavenging activity. DPPH scavenging activity was calculated using Eq. (2)

$$\% \text{ DPPH scavenging} = \frac{A_c - A_s}{A_c} \times 100 \quad (2)$$

Where the A_c –absorbance of the control and A_s - absorbance of the sample is [19].

2.3.4. Antimicrobial assay.

The prepared compounds were tested for their antimicrobial activity against Gram-negative bacteria (*Escherichia coli*) and Gram-positive bacteria (*Staphylococcus aureus*, *Bacillus subtilis*), as well as fungal strains (*Aspergillus niger* and *Candida albicans*). Standard antibiotics amoxicillin (25 mg) and fluconazole (25 mg) served as positive controls. The microbes were tested in terms of minimum inhibitory concentration (MIC) using a serial plate dilution assay [20]. Microbial cultures were incubated at 34°C for 24 h. Mueller-Hinton broth of bacteria (100 µL) was pipetted into each well, and 10 µL of the pathogen suspension was then added. 4% DMSO solution was used as a negative control to monitor the sample's sterility and assess the solvent's antimicrobial influence. Zone of inhibition was measured, and MIC was determined by double-fold serial dilution in liquid media containing varying concentrations of test samples ranging from 1 to 1000 µg/mL. The turbidity of the culture measured bacterial growth after 18h. McFarland Standard 0.5 was used as the turbidity standard [21].

3. Results and Discussion

3.1. Chemistry.

A new *N, N*-donor bidentate bioactive ligand (HL) and its Cu(II) and Ni(II) complexes were prepared following literature methods. The microelemental analyses for C, H, N, O, and M, and the molecular weights of the complexes, were in good agreement with the proposed structures of the complexes [22,23]. The analytical data were summarized, and the results are reliable compared with those calculated for the proposed formulae. The synthesized compounds were stable, non-hygroscopic, and soluble in organic solvents such as ethanol, DMF, and DMSO. The analytical data are depicted in Table 1 [24].

Table 1. Physical properties of the ligand (HL) and its metal complexes B-1 and B-2.

Compound	M.W (g/mol)	Color	M.P (°C)	Yield (%)	M:L	Elemental analysis				
						C	H	N	O	M
HL	277	Pink	122	89	-	56.29	6.91	25.25	11.53	-
B-1	652	Brown	149	91	1:2	54.27	5.89	18.61	12.75	8.45
B-2	648	Pale green	113	84	1:2	49.49	7.11	20.61	14.71	8.64

3.2. FT-IR spectra.

The IR spectrum of the ligand (HL) is compared with that of metal complexes to investigate the mode of binding between the ligand and the metal ions. The characteristic bands in the IR spectrum of the synthesized HL and the metal complexes are listed in Table 2 and Figure 1. The band at 1635 is assigned to (C=N-) stretching frequency. The bands at 3409 and 2894 cm^{-1} are due to the stretching of (-NH) and (-CH) groups, respectively. On complexation, the bands of the azomethine groups shift to lower wave numbers (1630 and 1624 cm^{-1}) compared to the imine ligand. Looking at the shifts and decreases in intensities before and after complexation, it is evident that these groups are involved in the complex formation. From the IR spectral data, it is known that HL behaves as a bidentate ligand. The IR spectral data are listed in Table 2 and shown in Figure 1 [25,26].

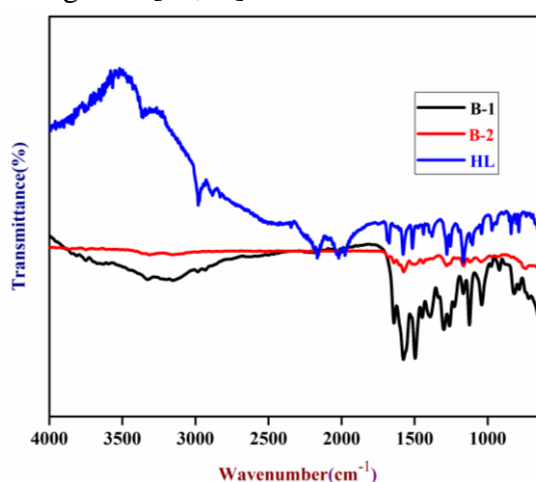


Figure 1. FT-IR spectra of HL and its metal complexes B-1 and B-2.

Table 2. FT-IR spectra of ligand (HL) and its metal complexes B-1 and B-2.

Compound	$\nu(\text{C}=\text{N})$	$\nu(\text{N}-\text{H})$	$\nu(\text{C}-\text{H})$	$\nu(\text{N}-\text{N})$	$\nu(\text{C}=\text{C})$	$\nu(\text{C}-\text{O})$	$\nu(\text{M}-\text{N})$
HL	1635	3409	2894	1156	1572	1287	-
B-1	1630	3090	2738	1041	1575	1241	673
B-2	1624	3189	2684	1051	1562	1225	691

3.3. UV/visible spectra.

The absorption spectra of HL and its metal complexes were recorded in dimethyl sulfoxide solution in the range of 300-800 nm. In the UV spectrum of the ligand, the absorption bands at 270 and 323 nm correspond to π - π^* and n - π^* transitions (Table 3, Figure 2). While the electronic spectrum $[\text{Cu}(\text{HL})_2] \times 2 \text{H}_2\text{O}$ and $[\text{Ni}(\text{HL})_2] \times 3\text{H}_2\text{O}$ complexes, displayed one band at 287 and 276 nm are attributed to n - π^* transitions and the bands at 319, 336 nm corresponds to π - π^* transition and the absorption bands at 406 nm and 368 nm corresponds to C-T transitions, respectively [27,28].

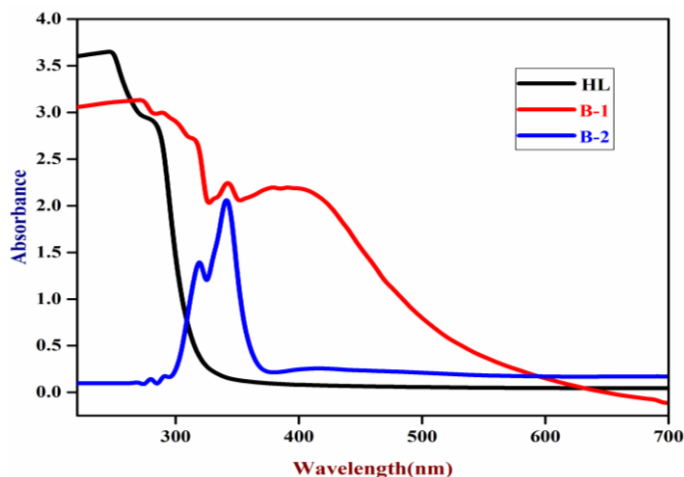


Figure 2. UV-Visible spectra of (HL) and its metal complexes B-1 and B-2.

Table 3. UV-Visible spectra of (HL) and its metal complexes B-1 and B-2.

Compound	π - π^*	n - π^*	C-T transition
HL	270 nm	323 nm	-
B-1	280 nm	340 nm	406 nm
B-2	293 nm	342 nm	368

3.4. NMR spectroscopy.

The ^1H NMR and ^{13}C NMR spectra of HL were shown in S1 and S2, respectively. A sharp singlet that integrates as one hydrogen at $\delta = 7.381$ ppm is assigned to azomethine ($-\text{CH}=\text{N}-$). The absence of coupling interactions due to the lack of protons on neighboring atoms results in singlet peaks for the imine protons. Another singlet at $\delta = 10.08$ ppm can be attributed to the proton attached to N. The multiplet signals of Ar-H were observed in the range 6.756 – 7.361 ppm. The structure of the ligand HL was further evaluated by ^{13}C NMR. The signals at $\delta = 153.92$ ppm are attributed to the carbon of azomethine. The peaks observed between $\delta = 110.945$ and 153.724 ppm correspond to aromatic ring carbons [29].

3.5. Mass spectroscopy.

The structure of the synthesized ligand (HL) and its metal complexes were confirmed through mass spectra. The mass spectrum of HL was shown in S3. The molecular ion peak is observed at $m/z = 278$ $[\text{M}+1]$, the molecular mass of the ligand (HL). The mass spectrum of the complexes showed molecular ion peaks at m/z 653 and 648 $[\text{M}+1]$, confirming the molecular masses of the complexes B-1 and B-2, as evident in S4 and S5, respectively [30].

3.6. Thermo-gravimetric analysis.

The complexes (B-1 and B-2) have been subjected to a temperature program in the range of 27°C to 800°C under inert temperature, with a heating rate of 10°C.

The thermal degradation of the complex B-1 begins with the elimination of two water molecules at 60°C to 165°C with a weight loss of 5.50 % (calc. 5.52%). Another decomposition peak at 320 to 410°C showed a weight loss of 84.98% (calc. 84.96%) as a result of the loss of coordinated organic moiety. Finally, the temperature above 410°C, the stable end product left behind as metal oxide [31-32].

The decomposition of the B-2 complex started with the loss of two water molecules with an endothermic peak at 68 -150°C, showing 5.45% weight loss [calc 5.55%] followed by the major weight loss of 85.31% [calc. 85.49%] refers to the decomposition of coordinated ligands at 330 and 440°C. The metal oxide, NiO, is obtained as a residue above 440°C [33]. The TGA and DTA plots of the complexes B-1 and B-2 are shown in Figures 3 and 4, respectively.

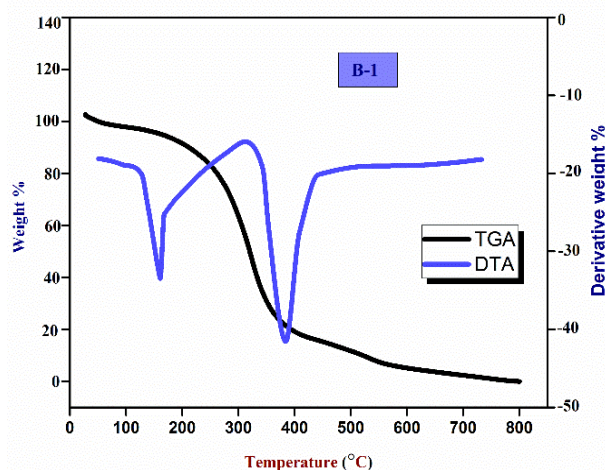


Figure 3. TGA and DTA plot of B-1 complex.

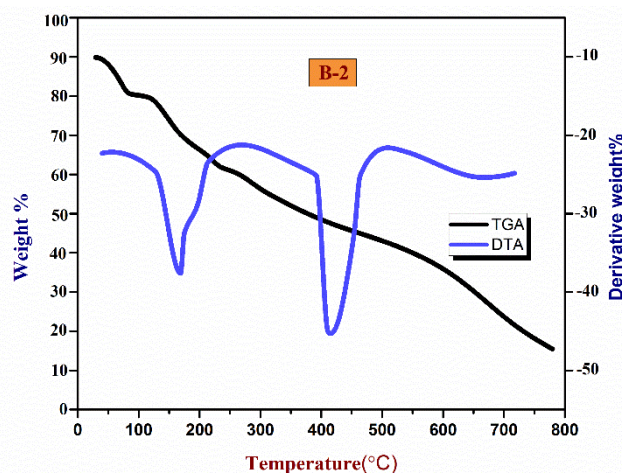


Figure 4. TGA and DTA plot of B-2 complex.

3.7. ESR spectra.

The magnetically active copper metal center was investigated by ESR spectroscopy, measured on an X-band spectrometer at liquid nitrogen temperature using DMSO as the solvent. ESR spectra of the copper complex are attributed to the coupling interaction of the unpaired electron with the copper nuclei. In the ESR spectrum, the small peaks and main bands

appear due to the delocalization of unpaired electrons on the nitrogen of the azomethine group via super-hyperfine interactions. The studies of the spectrum give $g_{\parallel} = 2.404$ and $g_{\perp} = 2.063$. This clearly indicates that $g_{\parallel} > g_{\perp} > 2.0023$ and the unpaired electron in Cu (II) resides in the dx^2-dy^2 orbital and is the characteristic spectral feature for axial symmetry (Figure 5). The complex has a distorted square planar geometry [34, 35].

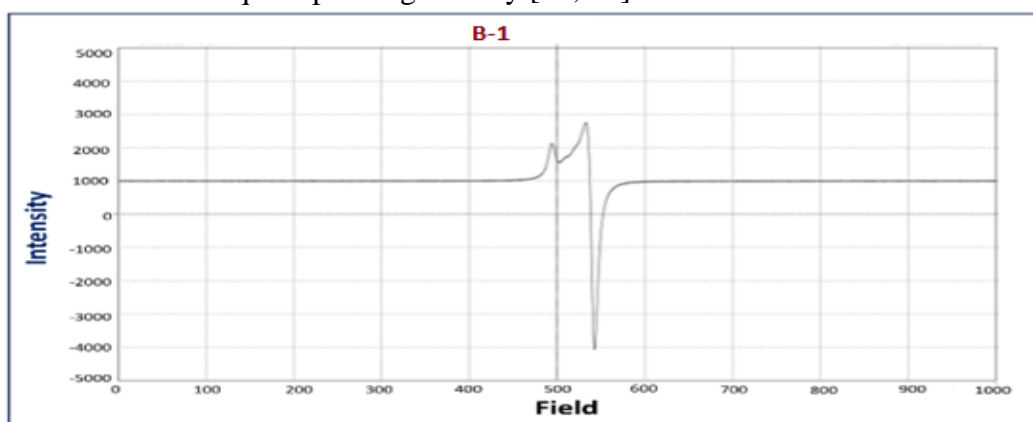
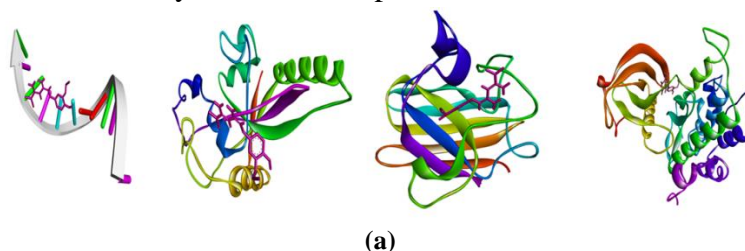


Figure 5. ESR spectrum of B-1 complex.

3.8. Molecular docking investigations.

The binding behavior of the compounds was analyzed by docking the pharmacologically active molecules into the protein's active sites. The binding interaction sites are available in the Discovery Studio visualizer. This calculation has been used to interpret how these proteins interact with small molecules. The interaction of DNA(1BNA), p53 cancer mutant protein (4L09), Cu, Zn-SOD(1CB4), and phosphorylated insulin receptor tyrosine kinase (2Z8C) with HL and its metal complexes B-1 and B-2, with docked energy parameters shown in Table IV and Figures 6, 7, and 8, respectively [36,37]. The ligand (HL) and its metal complexes B-1 and B-2 interact with DNA with the binding energies of -5.1, -6.4, and -5.9 kcal/mol, respectively. The interactions of HL and its metal complexes B-1 and B-2 with p53 cancer mutant protein with the binding scores of -5.9, -9.1 and -8.8 kcal/mol, and with Cu, Zn-SOD with the binding scores of -6.0, -6.3 and -6.2 kcal/mol and with phosphorylated insulin receptor, tyrosine kinase with the binding scores of -7.1, -6.6, and -8.8, respectively. These parameters indicate that the B-1 complex binds strongly to the p53 cancer mutant protein, followed by 2Z8C, 1CB4, and 1BNA. B-1 complex displayed the highest binding score of -9.1 kcal/mol with p53 cancer mutant protein, and the complex B-2 displayed the highest binding with phosphorylated insulin receptor tyrosine kinase 2Z8C. Docked compounds were analyzed based on hydrogen bonding, non-covalent, and hydrophobic interactions between 1BNA, 4L09,1CB4, and the synthesized compounds. The docking investigations revealed that the copper complex interacts more efficiently with the p53 cancer mutant protein, hydrolase enzyme, and DNA than other synthesized compounds [38].



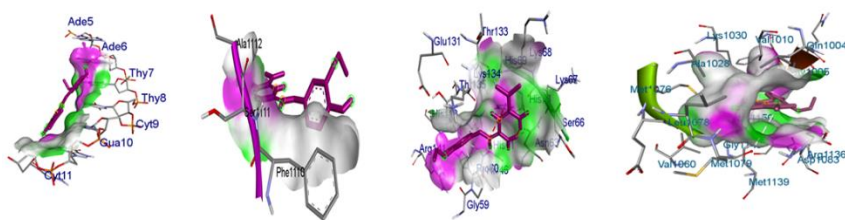
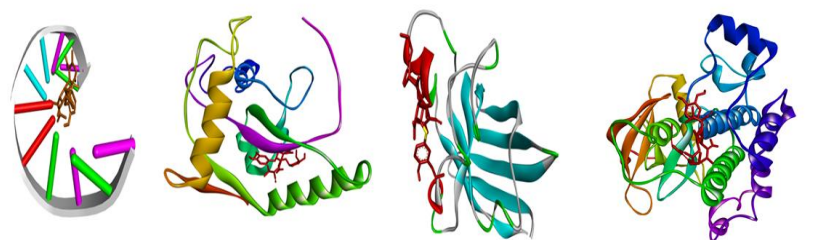
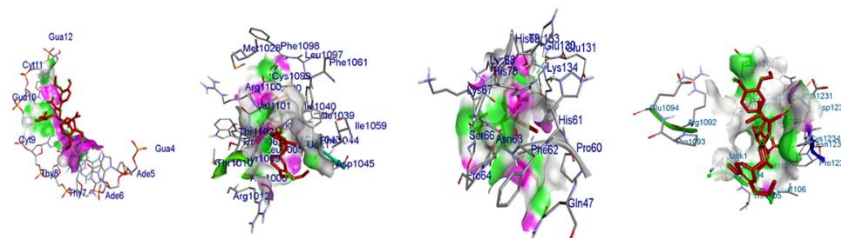


Figure 6. (a) Molecular docking of HL with 1BNA, 4L09, 1CB4, and 2Z8C; (b) Active site amino acid residues (1BNA, 4L09, 1CB4, and 2Z8C) interactions with HL.

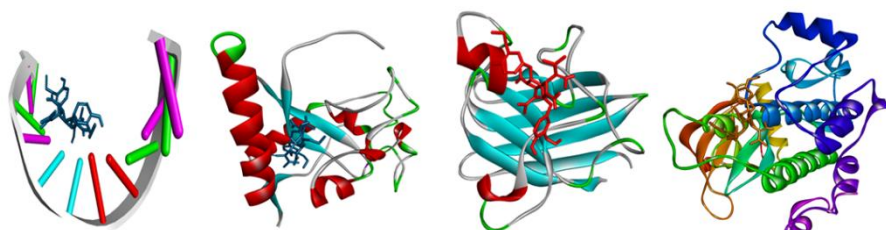


(a)

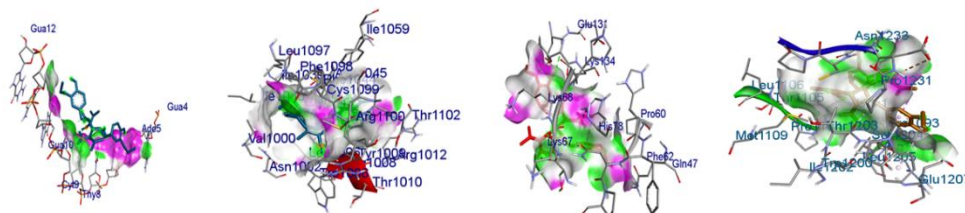


(b)

Figure 7. (a) Molecular docking of B-1 complex with 1BNA, 4L09, 1CB4 and 2Z8C(above); (b) Active site amino acid residues (1BNA, 4L09, 1CB4, and 2Z8C)interaction with B-1 complex(below).



(a)



(b)

Figure 8. (a) Molecular docking of B-2 complex with 1BNA, 4L09, 1CB4 and 2Z8C; (b) Active site amino acid residue (1BNA, 4L09, 1CB4, and 2Z8C) interactions with B-2 complex.

Table 4. Docking score of ligand (HL) and complexes B-1 and B-2.

Compound	Binding energy(kcal/mol)			
	1BNA	4L09	1CB4	2Z8C
HL	-5.1	-5.9	-6.0	-7.1
B-1	-6.4	-9.1	-6.3	-6.6
B-2	-5.9	-8.8	-6.2	-8.5

3.9. DNA binding studies.

3.9.1. Electronic absorption titrations.

Electronic absorption spectroscopy is used to determine the binding interaction of metal complexes with DNA. The UV-vis spectra of Cu(II) and Ni(II) complexes with CT-DNA are shown in Figures 9 and 10, respectively. The binding constant K_b for the complex has been determined from the plot of $[DNA]/(\epsilon a - \epsilon f)$ versus $[DNA]$ using equation (eq-1) and was found to be 3353.01 M^{-1} and 3263.06 M^{-1} for B-1 and B-2, respectively [39].

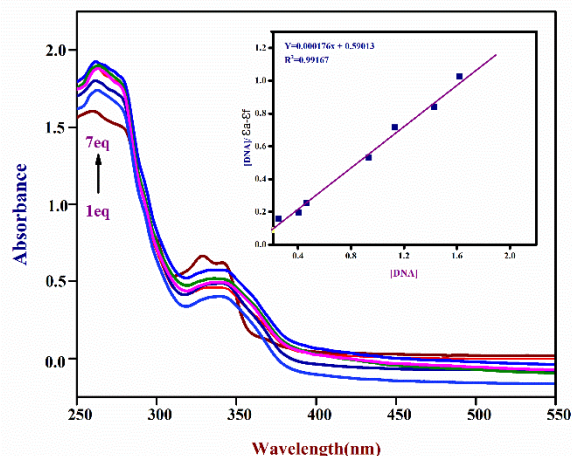


Figure 9. Absorption spectra of B-1 complex in the presence of CT-DNA in tris-HCl buffer (pH=7.4); Inset: The plot of $[DNA]/(\epsilon a - \epsilon f)$ versus $[DNA]$.

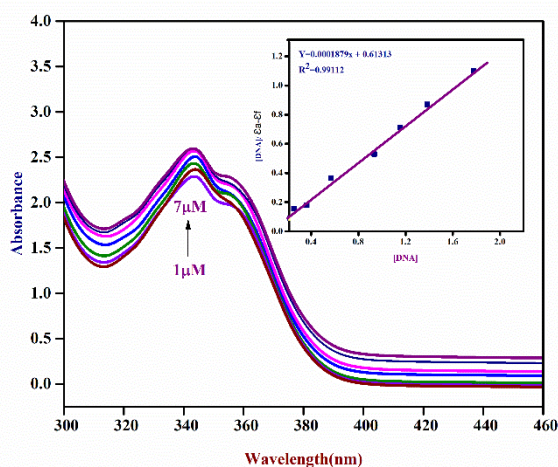


Figure 10. Absorption spectra of B-2 complex in the presence of CT-DNA in tris-HCl buffer (pH=7.4); Inset: The plot of $[DNA]/(\epsilon a - \epsilon f)$ versus $[DNA]$.

3.9.2. Fluorescence spectroscopic studies.

The fluorescence experiments were performed to investigate the interactions between ligands and CT-DNA complexes. The fluorescence spectra of the ligand showed no change in intensity upon the addition of CT-DNA. The fluorescence spectra of the complexes exhibited major peaks at 500 and 540 nm, respectively (Figures 11 and 12). Initially, the low fluorescence intensity was due to solvent quenching, and it gradually increased as it bound to DNA. As the concentration of the metal complexes increased, the emission intensity decreased slowly. The fluorescence emission intensities at 500 and 540 nm (excitation at 320 and 340 nm) decreased with increasing complex concentration. The quenching of fluorescence intensity of complexes by binding with CT-DNA was further used to determine the binding constant (K_b) from the <https://nanobioletters.com/>

plot of F_0/F versus $[Q]$ using the following equation [eq-3] and was found to be $7.028 \times 10^3 \text{ M}^{-1}$ and $5.921 \times 10^3 \text{ M}^{-1}$ [40] and the Stern-Volmer quenching constant (k_{sv}) Figure 13 and Figure 14, was obtained from the plot of $\log [(F_0-F)/F]$ versus $\log[Q]$ using the following equation (eq-4) and were found to be 2.674×10^3 and 2.102×10^3 . These results indicate that the Cu(II) complex binds to DNA more efficiently than the Ni(II) complex [41].

$$\frac{F_0}{\Delta F} = \frac{1}{fa} + \frac{1}{faKa} [Q] \quad (3)$$

$$\log\left(\frac{F_0-F}{F}\right) = \log k_b + n \log[Q] \quad (4)$$

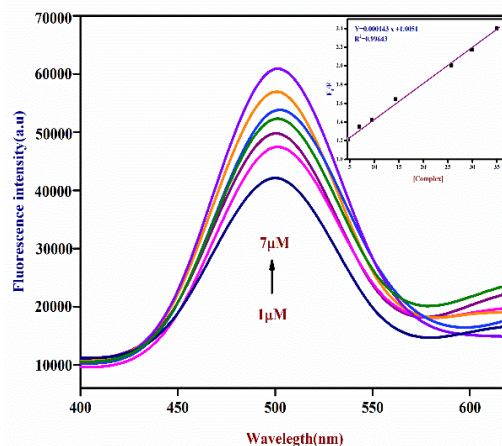


Figure 11. Emission spectra of B-1 complex in the presence of CT-DNA in tris-HCl buffer (pH=7.4) [$\lambda_{exc}=320\text{nm}$; $\lambda_{ems}=540\text{nm}$]; Inset: The plot of F_0/F v/s $[Q]$.

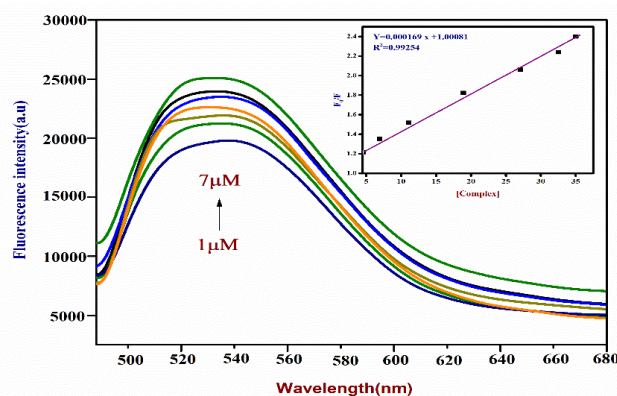


Figure 12. Emission spectra of B-2 complex in the presence of CT-DNA in tris-HCl buffer (pH=7.4) [$\lambda_{exc}=340\text{nm}$; $\lambda_{ems}=500\text{nm}$]; Inset: The plot of F_0/F v/s $[Q]$.

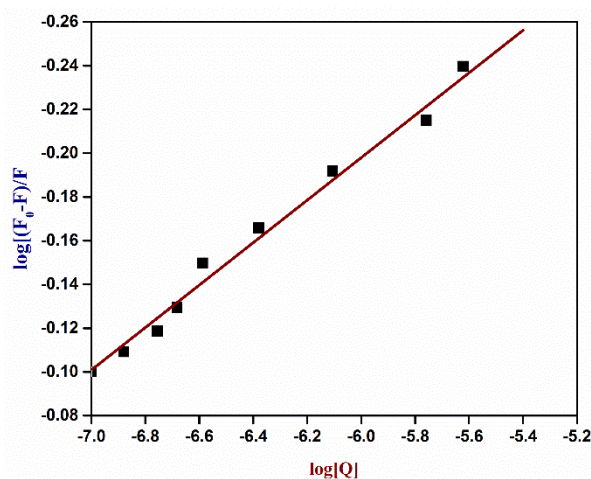


Figure 13. A plot of $\log[(F_0-F)/F]$ versus $\log[Q]$.

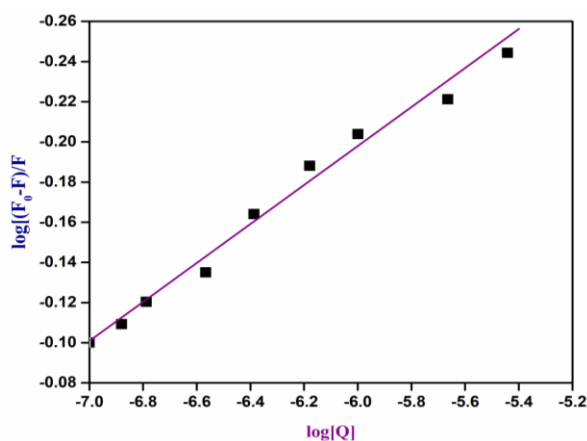


Figure 14. A plot of $\log[(F_0-F)/F]$ versus $\log[Q]$.

3.10. Pharmacological studies.

3.10.1. Evaluation of antioxidant activity.

The synthesized compounds showed lower scavenging activity compared to the standard. The antioxidant property of the ligand (HL) and its metal complexes is expressed as IC_{50} values depicted in Table 5. Among the synthesized compounds, Cu(II) complex showed the highest antioxidant activity, leading to a lower IC_{50} value, since the substituents /groups [electron-donating and electron-withdrawing groups] play a significant role in antioxidant activity. Figure 15 and Table 5 describe the inhibitory effects of HL and its metal complexes [B-1 and B-2] [42,43].

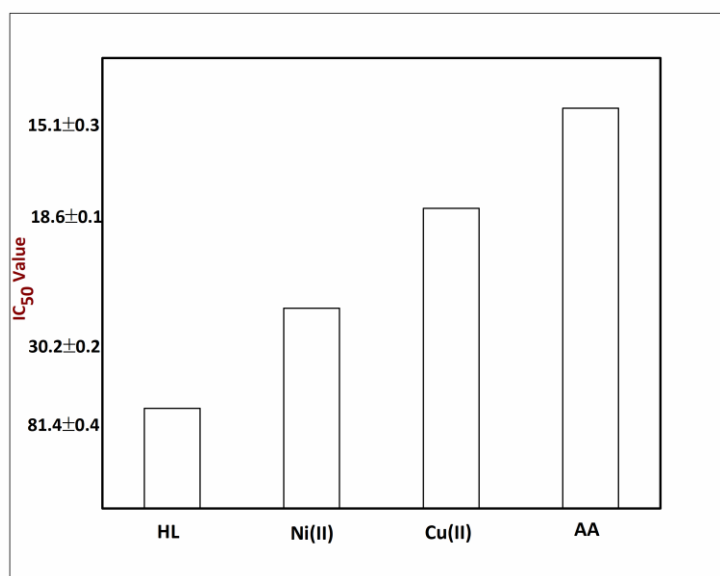


Figure 15. IC_{50} inhibitory concentrations of ligand (HL) and its metal complexes, B-1 and B-2, for 50 % of DPPH radical.

Table 5. 50% inhibitory concentrations (IC_{50}) of the radical scavenging activity of ligand (HL) and metal complexes B-1 and B-2.

Sl.No	Compound	IC_{50}
1	HL	81.4±0.4
2	B-1	18.6±0.1
3	B-2	30.2±0.2
4	AA	15.1±0.3

3.10.2. Antimicrobial activity.

The antimicrobial activities were screened using bacterial and fungal strains. The results were recorded as shown in Table 6. It is inferred that the Schiff base ligand and its metal complexes inhibited the growth of *B. subtilis*, *E. coli*, and *S. aureus* [44]. The susceptibility zones were measured in diameter (mm) and corresponded to the clear zones around the discs that killed bacteria and fungi. The ligand (HL) and its metal complexes exhibited varying degrees of inhibitory effects on the growth of the tested bacterial and fungal species. The metal complexes showed more antifungal activity than the parent ligand (HL). All of the investigated compounds produced fewer inhibition zones than the standard, as shown in Figure 16 and tabulated in Table 6 [45].

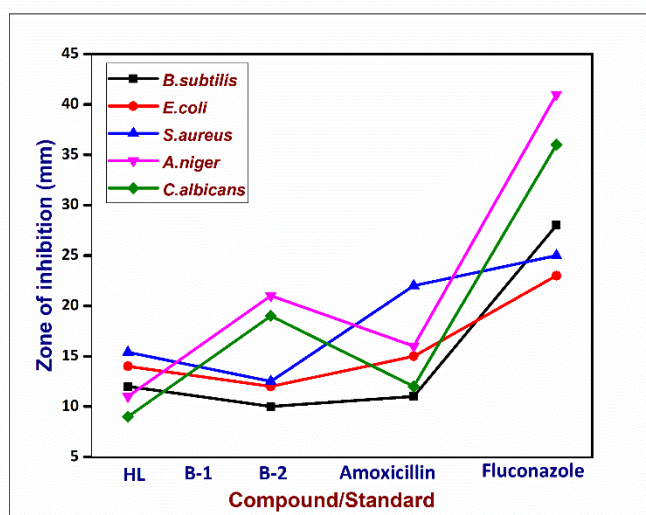


Figure 16. Graphical representation of the antimicrobial activity of HL and its metal complexes B-1 and B-2.

Table 6. Antimicrobial activity of ligand (HL) and its complexes B-1 and B-2.

Compound	Zone of Inhibition				
	Bacteria			Fungi	
	<i>B.Subtilis</i>	<i>E.Coli</i>	<i>S.Aureus</i>	<i>A.Niger</i>	<i>C.Albicans</i>
HL	12	14	15.4	11	09
B-1	10	12	12.5	21	19
B-2	11	15	22	16	12
Amoxicillin	28	23	25	-	-
Fluconazole	-	-	-	41	36

4. Conclusions

In the present study, Schiff base and its Copper and Nickel complexes were prepared and characterized by physicochemical methods. Elemental analysis reveals that the complexes have a metal-to-ligand ratio (1:2). FT-IR spectra support the coordination of ligand to metal through azomethine nitrogen and nitrogen of the amine group. ¹H-NMR, ¹³C-NMR, LC-MS, and FT-IR data support the structure of the ligand (HL) and the complexes. TGA provides a depiction of the degradation path and stability of the complexes formed. The presence of azomethine and amine groups in the ligand enhanced the antioxidant activity of the complexes. The antibacterial and antifungal activities reported in this paper indicate that the complex exhibited the highest antifungal activity compared to the ligand. Molecular docking studies indicate that the Cu(II) complex binds more effectively to the p53 cancer mutant protein than to DNA, the hydrolase enzyme, or the phosphorylated insulin receptor tyrosine kinase, with a good binding score.

Author Contributions

Conceptualization, P.M. and R.H.D.R.; methodology, P.M. and R.H.D.R.; software, P.M.; validation, P.M.; formal analysis, P.M.; investigation, R.H.D.R.; resources, P.M.; data curation, P.M.; writing—original draft preparation, P.M.; writing—review and editing, P.M. and R.H.D.R.; visualization, P.M.; supervision, R.H.D.R.; project administration, R.H.D.R. All authors have read and agreed to the published version of the manuscript.

Institutional Review Board Statement

Not applicable.

Informed Consent Statement

Not applicable.

Data Availability Statement

Data supporting the findings of this study are available upon reasonable request from the corresponding author.

Funding

This research work received no external funding.

Acknowledgments

The author, M Prema, is thankful to the UOM-OBC cell for awarding the fellowship and also extending thanks to the Institute of Excellence, Vijnan Bhavan, Mysuru, and IIT Bombay for Instrumental facilities.

Conflicts of Interest

The authors declare no conflict of interest.

References

1. Ismail, A.H.; Al-Garawi, Z.S.; Al-Shamari, K.; Salman, A.T. Metformin compounds: A review on the importance and the possible applications. *J. Phys.: Conf. Ser.* **2021**, *1853*, 012060, <https://doi.org/10.1088/1742-6596/1853/1/012060>.
2. Sharma, S.S.; Ramani, J.V.; Dalwadi, D.P.; Bhalodia, J.P.; Patel, N.K.; Patel, D.D.; Patel, R.K. New Ternary Transition Metal Complexes of 2-[(2-aminophenyl)imino] methyl}Phenol and Metformin: Synthesis, Characterization and Antimicrobial Activity. *J. Chem.* **2011**, *8*, 723491, <https://doi.org/10.1155/2011/723491>.
3. Al-Qadisy, I.; Saeed, W.S.; Al-Odayni, A.-B.; Ahmed Saleh Al-Faqeeh, L.; Alghamdi, A.A.; Farooqui, M. Novel Metformin-Based Schiff Bases: Synthesis, Characterization, and Antibacterial Evaluation. *Materials* **2020**, *13*, 514, <https://doi.org/10.3390/ma13030514>.
4. Mahmoud, M.A.; Abdel-Salam, E.T.; Abdel Aal, N.F.; Showery, Z.M.; Sallam, S.A. Dy(III) complexes of metformin Schiff-bases as glucose probe: synthesis, spectral, and thermal properties. *J. Coord. Chem.* **2019**, *72*, 749-769, <https://doi.org/10.1080/00958972.2019.1569642>.
5. Mahmoud, M.A.; Zaitone, S.A.; Ammar, A.M.; Sallam, S.A. Synthesis, structure and antidiabetic activity of chromium(III) complexes of metformin Schiff-bases. *J. Mol. Struct.* **2016**, *1108*, 60-70, <https://doi.org/10.1016/j.molstruc.2015.11.055>.

6. Stepensky, D.; Friedman, M.; Srour, W.; Raz, I.; Hoffman, A. Preclinical evaluation of pharmacokinetic–pharmacodynamic rationale for oral CR metformin formulation. *J. Control. Release* **2001**, *71*, 107-115, [https://doi.org/10.1016/S0168-3659\(00\)00374-6](https://doi.org/10.1016/S0168-3659(00)00374-6).
7. Subasinghe, S.; Greenbaum, A.L.; McLean, P. The insulin-mimetic action of Mn²⁺: Involvement of cyclic nucleotides and insulin in the regulation of hepatic hexokinase and glucokinase. *Biochem. Med.* **1985**, *34*, 83-92, [https://doi.org/10.1016/0006-2944\(85\)90064-X](https://doi.org/10.1016/0006-2944(85)90064-X).
8. Zhu, M.; Lu, L.; Yang, P.; Jin, X. Bis (1, 1-dimethylbiguanido) copper (II) octahydrate. *Acta Crystallogr., Sect. E: Struct. Rep. Online* **2002**, *58*, m217-m219, <https://doi.org/10.1107/S1600536802007092>.
9. Patrinoiu, G.; Patron, L.; Carp, O.; Stanica, N. Thermal Behaviour of Some Iron(III) Complexes with Active Therapeutically Biguanides. *J. Therm. Anal. Calorim.* **2003**, *72*, 489-495, <https://doi.org/10.1023/A:1024509228813>.
10. Olar, R.; Badea, M.; Cristurean, E.; Lazar, V.; Cernat, R.; Balotescu, C. Thermal behavior, spectroscopic and biological characterization of Co (II), ZN (II), Pd (II) And Pt (II) Complexes With N, N-Dimethylbiguanide. *J. Therm. Anal. Calorim.* **2005**, *80*, 451-455.
11. Al-Saif, F.A.; Refat, M.S. Synthesis, spectroscopic, and thermal investigation of transition and non-transition complexes of metformin as potential insulin-mimetic agents. *J. Therm. Anal. Calorim.* **2013**, *111*, 2079-2096, <http://dx.doi.org/10.1007/s10973-012-2459-3>.
12. Jaiganesh, C.; Subramanian, S. Metformin-3-hydroxyflavone, A New Schiff Base Complex Modulates the Activities of Carbohydrate Regulatory Enzymes in High Fat Diet Fed-Low Dose Streptozotocin Induced Type 2 Diabetes in Experimental Rats. *J. Chem. Pharm. Res.* **2017**, *9*, 90-100,
13. Koothappan, M.; Vellai, R.D.; Subramanian, I.P.; Subramanian, S.P. Synthesis of a New Zinc-Mixed Ligand Complex and Evaluation of Its Antidiabetic Properties in High Fat Diet: Low Dose Streptozotocin Induced Diabetic Rats. *Diabetes Metab. J.* **2018**, *42*, 244-248, <https://doi.org/10.4093/dmj.2018.0002>.
14. Mahmoud, M.; Abdel-Salam, E.; Abou-Elmagd, M.; Sallam, S. Template Synthesis, Spectral, Thermal and Glucose Sensing of Pr³⁺ Complexes of Metformin Schiff-Bases. *J. Fluoresc.* **2019**, *29*, 319-333, <https://doi.org/10.1007/s10895-018-02341-5>.
15. Dhananjayan, K. Molecular Docking Study Characterization of Rare Flavonoids at the Nac-Binding Site of the First Bromodomain of BRD4 (BRD4 BD1). *J. Cancer Res.* **2015**, *2015*, 762716, <https://doi.org/10.1155/2015/762716>.
16. Vijesh, A.M.; Isloor, A.M.; Telkar, S.; Arulmoli, T.; Fun, H.-K. Molecular docking studies of some new imidazole derivatives for antimicrobial properties. *Arab. J. Chem.* **2013**, *6*, 197-204, <https://doi.org/10.1016/j.arabjc.2011.10.007>.
17. Sunita, M.; Anupama, B.; Ushaiah, B.; Gyana Kumari, C. Synthesis, characterization, DNA binding and cleavage studies of mixed-ligand copper (II) complexes. *Arab. J. Chem.* **2017**, *10*, S3367-S3374, <http://dx.doi.org/10.1016/j.arabjc.2014.01.017>.
18. Tadele, K.T. Antioxidant Activity of Schiff Bases and Their Metal Complexes: A Recent Review. *J. Pharm. Med. Res.* **2017**, *3*, 73–77.
19. Vairalakshmi, M.; Princess, R.; Raja, S.J. THE METAL COMPLEXES OF NOVEL SCHIFF BASE CONTAINING ISATIN: CHARACTERIZATION, ANTIMICROBIAL, ANTIOXIDANT AND CATALYTIC ACTIVITY STUDY. *Asian J. Pharm. Clin. Res* **2019**, *12*, 206-210, <https://doi.org/10.22159/ajpcr.2019.v12i18.34189>.
20. Zalevskaya, O.A.; Gur'eva, Y.A. Recent Studies on the Antimicrobial Activity of Copper Complexes. *Russ. J. Coord. Chem.* **2021**, *47*, 861-880, <https://doi.org/10.1134/S1070328421120046>.
21. Bisceglie, F.; Bacci, C.; Vismarra, A.; Barilli, E.; Pioli, M.; Orsoni, N.; Pelosi, G. Antibacterial activity of metal complexes based on cinnamaldehyde thiosemicarbazone analogues. *J. Inorg. Biochem.* **2020**, *203*, 110888, <https://doi.org/10.1016/j.jinorgbio.2019.110888>.
22. Yousif, E.; Majeed, A.; Al-Sammarrae, K.; Salih, N.; Salimon, J.; Abdullah, B. Metal complexes of Schiff base: Preparation, characterization and antibacterial activity. *Arab. J. Chem.* **2017**, *10*, S1639-S1644, <https://doi.org/10.1016/j.arabjc.2013.06.006>.
23. Jabbi, A.M.; Aliyu, H.N.; Isyaku, S.; Kabir, A.M. Preparation, Characterization and Antimicrobial Studies of Mn(II) and Fe(II) Complexes with Schiff Base Ligand Derived from 2-aminophenol and 3-formyl-2-hydroxy-6-methoxyquinoline. *Open J. Inorg. Chem.* **2020**, *10*, 15-24, <https://doi.org/10.4236/ojic.2020.102003>.

24. Ado, I.; Na'Aliya, J.; Sani, S.; Haleelu, M.M. Synthesis, spectroscopic and antimicrobial studies of Co (II), Ni (II), Cu (II) and Zn (II) complexes derived from benzoic acid bidentate Schiff base ligand. *J. Appl. Sci. Environ. Manage.* **2021**, *25*, 1599-1603, <https://doi.org/10.4314/jasem.v25i9.9>.
25. Yusuf, T.L.; Oladipo, S.D.; Zamisa, S.; Kumalo, H.M.; Lawal, I.A.; Lawal, M.M.; Mabuba, N. Design of New Schiff-Base Copper(II) Complexes: Synthesis, Crystal Structures, DFT Study, and Binding Potency toward Cytochrome P450 3A4. *ACS Omega* **2021**, *6*, 13704-13718, <https://doi.org/10.1021/acsomega.1c00906>.
26. Sumathi, R.B.; Halli, M.B. Metal (II) Complexes Derived from Naphthofuran-2-carbohydrazide and Diacetylmonoxime Schiff Base: Synthesis, Spectroscopic, Electrochemical, and Biological Investigation. *Bioinorg. Chem. Appl.* **2014**, *2014*, 942162, <https://doi.org/10.1155/2014/942162>.
27. Vinusha, H.M.; Kollur, S.P.; Revanasiddappa, H.D.; Ramu, R.; Shirahatti, P.S.; Nagendra Prasad, M.N.; Chandrashekar, S.; Begum, M. Preparation, spectral characterization and biological applications of Schiff base ligand and its transition metal complexes. *Res. Chem.* **2019**, *1*, 100012, <https://doi.org/10.1016/j.rechem.2019.100012>.
28. Jeslin Kanaga Inba, P.; Annaraj, B.; Thalamuthu, S.; Neelakantan, M.A. Cu(II), Ni(II), and Zn(II) Complexes of Salan-Type Ligand Containing Ester Groups: Synthesis, Characterization, Electrochemical Properties, and In Vitro Biological Activities. *Bioinorg. Chem. Appl.* **2013**, *2013*, 439848, <http://dx.doi.org/10.1155/2013/439848>.
29. Abd-Elzaher, M.M.; Labib, A.A.; Mousa, H.A.; Moustafa, S.A.; Ali, M.M.; El-Rashedy, A.A. Synthesis, anticancer activity and molecular docking study of Schiff base complexes containing thiazole moiety. *Beni-Suef Univ. J. Basic Appl. Sci.* **2016**, *5*, 85-96, <http://dx.doi.org/10.1016/j.bjbas.2016.01.001>.
30. Deepika, P.; Vinusha, H.M.; Begum, M.; Ramu, R.; Shirahatti, P.S.; Nagendra Prasad, M.N. 2-methoxy-4-(((5-nitropyridin-2-yl)imino)methyl)phenol Schiff base ligand and its Cu(II) and Zn(II) complexes: synthesis, characterization and biological investigations. *Heliyon* **2022**, *8*, e09648, <https://doi.org/10.1016/j.heliyon.2022.e09648>.
31. Manjuraj, T.; Yuvaraj, T.C.M.; Jayanna, N.D.; Sarvajith, M.S. Design, spectral, thermal, DFT studies, antioxidant and molecular docking studies of pyrazole-based schiff base ligand and its metal (II) complexes. *Mater. Today: Proc.* **2022**, *54*, 646-655, <https://doi.org/10.1016/j.matpr.2021.10.354>.
32. Jayaseelan, P.; Prasad, S.; Vedanayaki, S.; Rajavel, R. Synthesis, characterization, anti-microbial, DNA binding and cleavage studies of Schiff base metal complexes. *Arab. J. Chem.* **2016**, *9*, S668-S677, <https://doi.org/10.1016/j.arabjc.2011.07.029>.
33. Gurnule, W.B.; Rathod, Y.U.; Belsare, A.D.; Das, N.C. Thermal degradation and antibacterial study of transition metal complexes derived from novel terpolymer ligand. *Mater. Today: Proc.* **2020**, *29*, 1044-1049, <https://doi.org/10.1016/j.matpr.2020.04.708>.
34. Mruthyunjayaswamy, B.H.M.; Ijare, O.B.; Jadegoud, Y. Synthesis, characterization and biological activity of symmetric dinuclear complexes derived from a novel macrocyclic compartmental ligand. *J. Braz. Chem. Soc.* **2005**, *16*, 783-789, <https://doi.org/10.1590/S0103-50532005000500016>.
35. Amonovich, T.M.; Nematovna, S.D.; Giyasovich, A.K.; Bafayevich, U.B.; Shukurullayevich, G.B.; Qizi, S.N.Q. Synthesis and ESR Spectroscopy Complexes of Copper (II) with Acyl-and Aroylhydrazones of Methyl Ester of 5, 5-Dimethyl-2, 4-Dioxohexanoic Acid. *Am. J. Org. Chem.* **2020**, *6*, 24-29, <https://doi.org/10.11648/J.AJHC.20200602.12>.
36. Hassanin, H.M.; Serya, R.A.T.; Abd Elmoneam, W.R.; Mostafa, M.A. Synthesis and molecular docking studies of some novel Schiff bases incorporating 6-butylquinolinedione moiety as potential topoisomerase II β inhibitors. *R. Soc. Open Sci.* **2018**, *5*, 172407, <https://doi.org/10.1098/rsos.172407>.
37. Zabiulla; Kouser, S.; Joythi, M.; Bushra Begum, A.; Asha, M.S.; Hezam Al-Ostoot, F.; Lakshmeesha, D.P.; Ramu, R.; Ara Khanum, S. Molecular docking, synthesis and antimicrobial evaluation of metal complexes with Schiff base. *Res. Chem.* **2023**, *5*, 100650, <https://doi.org/10.1016/j.rechem.2022.100650>.
38. John, L.; Joseyphus, R.S.; Joe, I.H. Biomedical application studies of Schiff base metal complexes containing pyridine moiety: molecular docking and a DFT approach. *SN Appl. Sci.* **2020**, *2*, 500, <https://doi.org/10.1007/s42452-020-2274-6>.
39. Chandrasekar, T.; Arunadevi, A.; Raman, N. Synthesis, spectral characterization, DNA-binding and antimicrobial profile of biological active mixed ligand Schiff base metal(II) complexes incorporating 1,8-diaminonaphthalene. *J. Coord. Chem.* **2021**, *74*, 804-822, <https://doi.org/10.1080/00958972.2020.1870967>.
40. Srivastava, V.K. Synthesis, characterization, and biological studies of some biometal complexes. *Future J. Pharm. Sci.* **2021**, *7*, 51, <https://doi.org/10.1186/s43094-021-00191-w>.

41. Saini, A.; Bansal, P. Quenching Studies as Important Toolkit For Exploring Binding Propensity of Metal Complexes with Serum Albumin and DNA (A Review). *Pharm. Chem. J.* **2022**, *56*, 545-558, <https://doi.org/10.1007/s11094-022-02676-1>.
42. Shah, S.S.; Shah, D.; Khan, I.; Ahmad, S.; Ali, U.; Rahman, A. Synthesis and Antioxidant Activities of Schiff Bases and Their Complexes: An Updated Review. *Biointerface Res. Appl. Chem* **2020**, *10*, 6936-6963, <https://doi.org/10.33263/BRIAC106.69366963>.
43. Gull, P.; Malik, M.A.; Dar, O.A.; Hashmi, A.A. Design, synthesis and characterization of macrocyclic ligand based transition metal complexes of Ni(II), Cu(II) and Co(II) with their antimicrobial and antioxidant evaluation. *J. Mol. Struct.* **2017**, *1134*, 734-741, <https://doi.org/10.1016/j.molstruc.2017.01.033>.
44. Bamigboye, M.O.; Ejidike, I.P.; Osunniran, W.A.; Adetunji, J.B.; Obaleye, J.A.; Adenipekun, C.A. Synthesis, characterization, antibacterial and toxicological studies of heteroleptic acetylsalicylic acid and anthranilic acid metal complexes. *J. Fundam. Appl. Sci.* **2023**, *15*, 62-82.
45. Salihović, M.; Pazalja, M.; Mahmutović-Dizdarević, I.; Jerković-Mujkić, A.; Suljagić, J.; Špirtović-Halilović, S.; Šapčanin, A. Synthesis, dft study and antimicrobial activity of schiff bases derived from benzaldehydes and amino acids. *Rasayan J. Chem.* **2018**, *11*, 1074–1083, <http://dx.doi.org/10.31788/RJC.2018.1133077>.

Publisher's Note & Disclaimer

The statements, opinions, and data presented in this publication are solely those of the individual author(s) and contributor(s) and do not necessarily reflect the views of the publisher and/or the editor(s). The publisher and/or the editor(s) disclaim any responsibility for the accuracy, completeness, or reliability of the content. Neither the publisher nor the editor(s) assume any legal liability for any errors, omissions, or consequences arising from the use of the information presented in this publication. Furthermore, the publisher and/or the editor(s) disclaim any liability for any injury, damage, or loss to persons or property that may result from the use of any ideas, methods, instructions, or products mentioned in the content. Readers are encouraged to independently verify any information before relying on it, and the publisher assumes no responsibility for any consequences arising from the use of materials contained in this publication.

Supplementary Materials

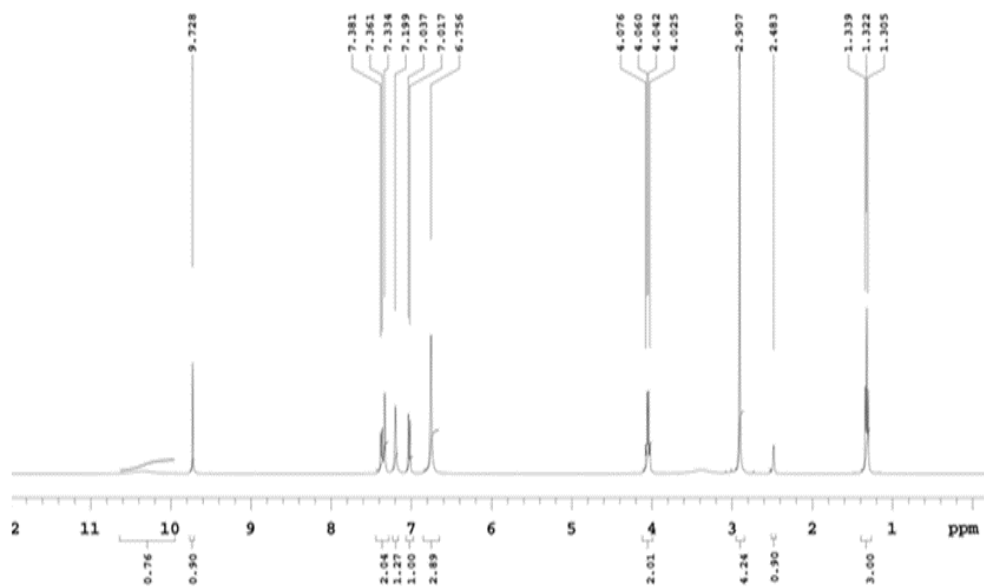


Figure S1. ¹H-NMR spectrum of HL.

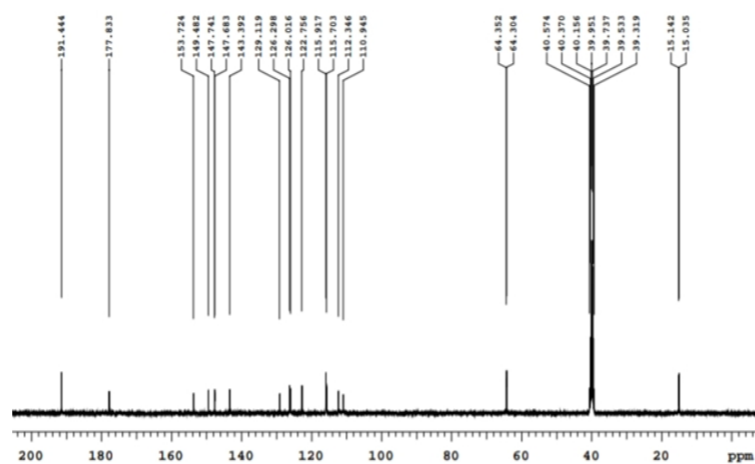


Figure S2. ¹³C-NMR spectrum of HL.

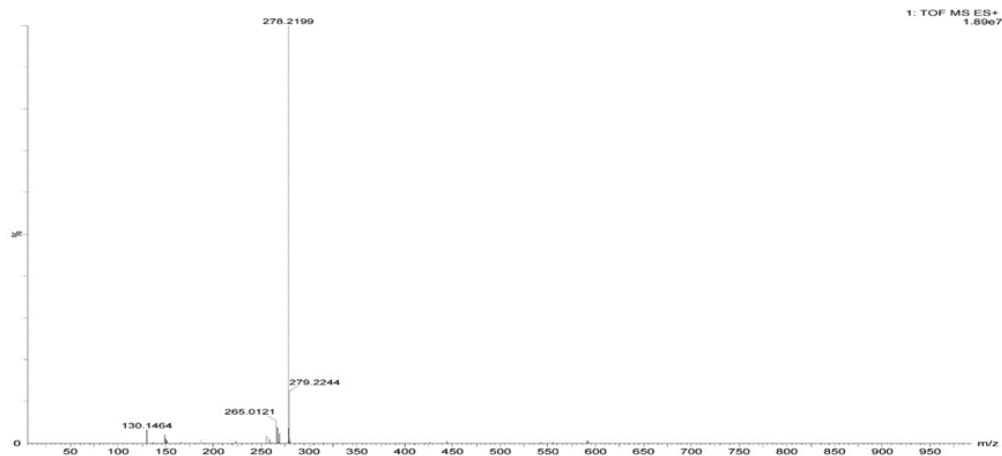


Figure S3. Mass spectrum of HL.

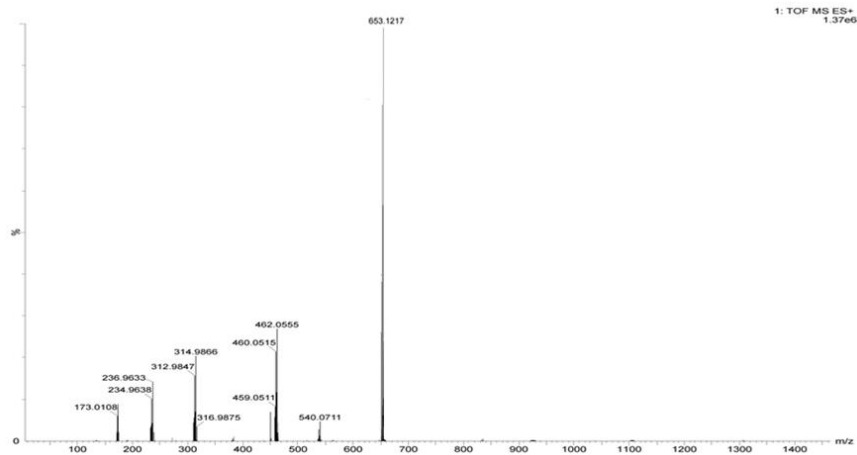


Figure S4. Mass spectrum of B-1 complex.

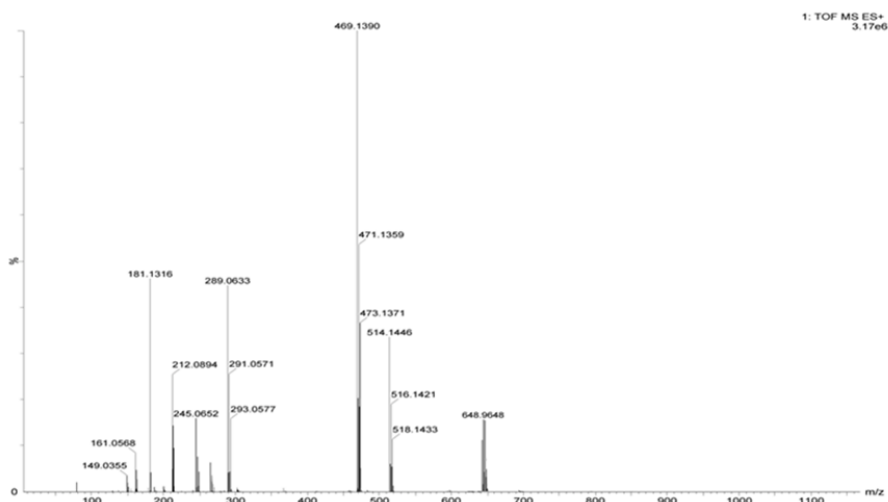


Figure S5. Mass spectrum of B-2 complex.